Journal of MATERIALS RESEARCH

Article
DOI: 10.1557/jmr.2019.386

Scale-dependent pop-ins in nanoindentation and scale-free plastic fluctuations in microcompression

John Shimanek[1], Quentin Rizzardi[1], Gregory Sparks[1], Peter M. Derlet[2], Robert Maaß[1,a)]

[1]Department of Materials Science and Engineering and Frederick Seitz Materials Research Laboratory, University of Illinois at Urbana-Champaign, Urbana, Illinois 61801, USA
[2]Condensed Matter Theory Group, Paul Scherrer Institute, Villigen-PSI 5232, Switzerland
[a)]Address all correspondence to this author. e-mail: rmaass@illinois.edu

Received: 2 July 2019; accepted: 3 December 2019

Nanoindentation and microcrystal deformation are two methods that allow probing size effects in crystal plasticity. In many cases of microcrystal deformation, scale-free and potentially universal intermittency of event sizes during plastic flow has been revealed, whereas nanoindentation has been mainly used to assess the stress statistics of the first pop-in. Here, we show that both methods of deformation exhibit fundamentally different event-size statistics obtained from plastic instabilities. Nanoindentation results in scale-dependent intermittent microplasticity best described by Weibull statistics (stress and magnitude of the first pop-in) and lognormal statistics (magnitude of higher-order pop-ins). In contrast, finite-volume microcrystal deformation of the same material exhibits microplastic event-size intermittency of truncated power-law type even when the same plastic volume as in nanoindentation is probed. Furthermore, we successfully test a previously proposed extreme-value statistics model that relates the average first critical stress to the shape and scale parameter of the underlying Weibull distribution.

Introduction

Discrete plastic flow is a well-known feature in both bulk deformation and microplasticity [1]. At the macroscopic scale, plastic instabilities during dynamic strain aging of solid solutions [2, 3] or serrated stress–strain behavior of complex multicomponent (high-entropy) alloys [4] and metallic glasses [5] can be observed. Only a small number of reports have revealed the intermittent nature of plastic flow via direct recording of discrete stress–strain curves obtained from pure bulk single crystals [6, 7, 8]. This is quite different at the small scale, where virtually any pure single-crystalline metal exhibits intermittent flow in a uniaxial deformation experiment [1, 9], which in contrast to bulk deformation may be due to the typically used deformation rates that are well below the underlying dislocation avalanche velocity [10]. The general observation of intermittent plastic flow also applies to a large number of nanoindentation studies that focus on incipient plasticity via so-called pop-ins [11, 12, 13, 14, 15, 16]. The main feature distinguishing the pop-ins of nanoindentation from the intermittent plasticity of microcrystal deformation is that the discrete plastic events of the latter are traced along the entire strain range, whereas pop-ins become unresolvable for large indentation depths. Consequently, pop-in statistics in nanoindentation have primarily been reported and analyzed for the first resolvable plastic instability. This means that stress–strain discontinuities probed in microcrystal deformation typically originate from the response of an already existing dislocation network, whereas sufficiently small nanoindentation tips are able to probe heterogeneous dislocation nucleation, as has been discussed intensely in the literature [14, 17, 18, 19, 20, 21]. As such, both techniques are able to probe size effects in plasticity, where the specimen size is varied in the case of microcrystal testing and the indenter tip size is varied in nanoindentation to probe a size effect related to the stressed volume underneath the tip [22]. Assessing the statistics of the first pop-ins with different tip sizes, one finds a similar change in the variability of stresses at which instabilities occur as when sampling the yield stress across specimen size (or dislocation density in samples of similar size) in microcrystal plasticity [18].

A popular statistical approach to evaluate the intermittent plastic response of microcrystals is the extraction of displacement jump sizes S from the force–displacement data and

subsequent representation in the form of probability density distributions $P_{int}(S)$, where the subscript *int* indicates that the distribution includes values of S for all stresses (stress-integrated distribution) [23, 24, 25, 26]. Much of this work has focused on power laws or truncated power laws that capture P_{int}, and has led to two fundamental implications: (i) (micro) plasticity is universal due to a very similar scaling exponent across a large range of different materials [27, 28, 29, 30], and (ii) intermittent (micro)plasticity lacks a particular microstructural length scale. Implication (i) suggests that intermittent flow is insensitive to material specifics, loading geometry, and microstructure, even though a number of recent reports advocate for nontrivial scaling exponents and, therefore, statistical data sets that are very much dependent on both experimental and microstructural details [10, 31, 32, 33, 34, 35].

In contrast to microcrystal deformation, statistical assessment of displacement instabilities (pop-ins) in nanoindentation has been limited to the first event and the shear stress at which it occurs. One reason for this is the complex geometry and stress state underneath the indentation tip, which makes the interpretation of a pop-in magnitude and stress less straightforward than in a uniaxial deformation experiment. Despite this, a very general extreme-value statistics approach [36] is able to predict the stress-magnitude statistics of the first pop-in seen in nanoindentation experiments as a function of indenter radius [22]. However, in view of the potentially universal aspect of intermittent plasticity, this complexity should not affect the actual scaling of the displacement magnitude distribution, but only nonuniversal pre-factors or the truncation term, as has been discussed in the context of loading-mode dependent event-size statistics [24, 37]. A second reason for focusing on the first pop-in in nanoindentation is the ability to probe dislocation nucleation or the activation of strong dislocation sources, whereas any subsequent events are clearly linked to the activation of the created network underneath the indenter tip. One would, thus, expect a change in distribution along the sequence of occurring pop-ins.

Here, we aim at investigating the size and stress statistics of plastic instabilities from the same prototypical Cu single crystal during both indentation and microcrystal deformation. We focus on the statistics of not only the first pop-in, but also higher-order events from nanoindentation with different tip sizes. The aim is to assess if scale-free and/or universal avalanche statistics are present in both types of microplastic flow, and how the statistical signature may change with event order.

We find that the statistics of event sizes in nanoindentation is scale-dependent, which is in direct contrast to finite-volume and scale-free intermittency in microcrystal deformation. Pop-in magnitudes of the first event follow a Weibull distribution, whereas higher-order events are distributed lognormally. The stress statistics are of Weibull type in both modes of deformation, with significant stress-scale mismatches. Finally, we also successfully test a recently proposed extreme-value statistics approach [36] for the stress statistics of the first pop-in in nanoindentation.

Results and discussion

In the following, we focus on the statistics of the first ten pop-ins as shown in Fig. 1. More specifically, we will separately consider the displacement statistics and stress statistics. Due to the complex stress state underneath the indentation tip, only the stress scale of the first pop-in per indent can be analyzed, whereas the displacement jump size of all ten tracked pop-ins will be discussed.

Displacement statistics

The displacement jump size of all considered pop-ins is summarized in a histogram in Fig. 2. In tip-size order, the data sets include approximately 7300, 8200, and 4700 analyzed events. It is seen that the data are bimodal for all three tip sizes and that there is a considerable change in scale of the first pop-in (#1) size in comparison to the higher-order events (#2–#10). Furthermore, pop-in sizes of event order #1 obtained with the smallest tip are distinctly smaller than those for the two larger indentation tips: first-order pop-ins initiated with the smallest tip never exceed 80 nm, whereas both larger tips generate distributions of event order #1 that have tails extending to 250 nm or more.

In contrast to the distinct scale mismatch of the first pop-ins, all higher-order events (#2–#10) are distributed similarly for all tip sizes, never exceeding 5 nm. While this is not shown in more detail here, there is no quantifiable difference between the statistical distributions of any higher-order event (e.g., event 2 versus event 3, or 4 versus 7) for the same tip size, indicating that once a dislocation structure has been formed underneath the indent, any subsequent collective dislocation activity that leads to pop-ins is of a statistically similar net displacement, as recorded with the axial displacement sensor. Among the three probe sizes, there is thus only a clear measurable size effect in the first pop-in, which indicates that a collective dislocation event underlying the abrupt displacement increment for event order #1 involves a much larger number of dislocations that exit the free surface. This is understood as a simple volume-scaling effect, where the length scale of the first event is set by the indentation tip size relative to the initial dislocation mean spacing and all subsequent events are determined by the newly introduced dislocation structure under the indentation tip. The observed similarity between the medium and large probe size will be addressed below in the context of Fig. 3.

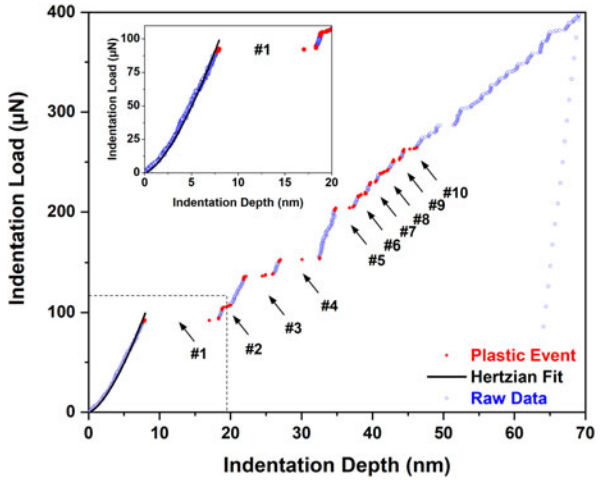

Figure 1: Indentation curve obtained with a tip size of 1.2 μm indicating in red the first identified pop-in events of orders #1–#10. The first part of the load–depth curve was fit with a Hertzian contact model, as highlighted in the inset.

A more quantitative method to examine the distributions describing the data seen in Fig. 2 is to test different distribution functions. This is done by evaluating complementary cumulative distribution functions (CCDFs) of that data, as displayed in Fig. 3, against a power law, a truncated power law, a stretched exponential (Weibull), and a lognormal distribution using the maximum likelihood estimator (MLE) method [38, 39]. The distribution equations are as follows:

$$\mathrm{CCDF}(x) \propto \mathrm{e}^{-(x/\lambda)^{\beta}} \quad , \tag{1}$$

for the Weibull distribution;

$$\mathrm{CCDF}(x) = \frac{1}{2}\left(1 - \mathrm{erf}\left[\frac{\ln x - \mu}{\sqrt{2}\sigma}\right]\right) \quad , \tag{2}$$

for the lognormal distribution; and

$$\mathrm{CCDF}(x) \propto x^{-\tau}\mathrm{e}^{-x/x_0} \quad , \tag{3}$$

for the truncated power law distribution.

These types of distributions are well-known functional forms used to quantify stress and event-size distributions [32, 36, 40, 41, 42]. It is found that the distribution of event sizes of order #1 from tests of all 3 tip sizes is best described with a Weibull distribution. Table I lists the relevant parameters, as determined by the MLE method, for the various CCDF distributions of both event #1 and the higher-order events.

The CCDFs for first-order events displayed in Fig. 3 reveal a non-monotonous order with tip size, where the data for the largest tip falls in-between the small and medium-sized probe. Subsequent atomic-force microscopy (AFM) analysis relates this to nanoscale asperities on the nominally conospherical tip, as shown in the inset of Fig. 3. For the largest tip, the first pop-ins typically occur at an indent depth of 30–40 nm, i.e., the yellow–green shaded area on the 3D color-mapped plot. The AFM-generated tip surface evidences an asperity that is ~10 nm taller than the main tip end. We thus conclude that the nominally large 50-μm tip has an effectively smaller radius (albeit the nominal radius will be referred to in the reminder of this document). Without this interfering effect, the size of the first pop-in would be expected to increase with increasing tip radius [43], which is indeed observed when comparing the two smaller tips that do not have any surface irregularities. It is noted that the "ridged" features seen in the inset of Fig. 3 are an artifact of minor vertical drift between individual AFM scan lines that are parallel to the *y*-axis.

Analysing the statistics of events #2–#10 shows that there is no change in distribution function across orders, allowing all higher-order events to be merged into one data set per tip size. The distributions for all tip sizes are found to be best described by a lognormal function, as summarized in Fig. 4.

Clearly, the statistical scaling of the events sizes observed with nanoindentation is distinctly different from event-size statistics in microcrystal deformation (deformed at 6 nm/s), where generally a power law or truncated power law is the favored distribution [1, 29, 44]. In the present case, a scaling exponent for the stress-integrated probability density distribution of 1.7 is found, which is lower than the value of 2 expected from mean field theory [29]. Furthermore, event sizes obtained from intermittent microcrystal plasticity do not change the distribution type with change of event order or strain but may exhibit a power law scaling exponent that is sensitive to stress scale (tuned criticality) [27]. Before discussing this difference in distribution further, an important experimental aspect needs to be considered: the statistical distribution of event sizes obtained from fluctuations in plasticity can be subject to changes if the sampling rate is too low, as shown by LeBlanc et al. [45]. It is thus of importance to verify that the lognormal distribution for events #2–#10 in Fig. 4 is not a result of under-sampling the deformation response. This can be conveniently interrogated by down-sampling the intermittent deformation response of the Cu microcrystals, which was acquired at a rate of 8 kHz, and to again conduct an MLE analysis of the much reduced data set. In doing so, it is found that a truncated power law remains with mathematical and statistical significance (significance value $P \ll 0.05$; likelihood ratio $R \gg 1$ for a truncated power law) the best suited functional form to describe the 20-Hz down-sampled microcrystal data. Now being sampled at the same rate as the nanoindentation experiments, no change in distribution is observed, but the number of small events reduces and the uncertainty for the obtained scaling exponents τ and the nonuniversal factor x_0 in the truncation term increases. This is expected because the full data set reduces from ~300 data points to ~120. We can, therefore, conclude

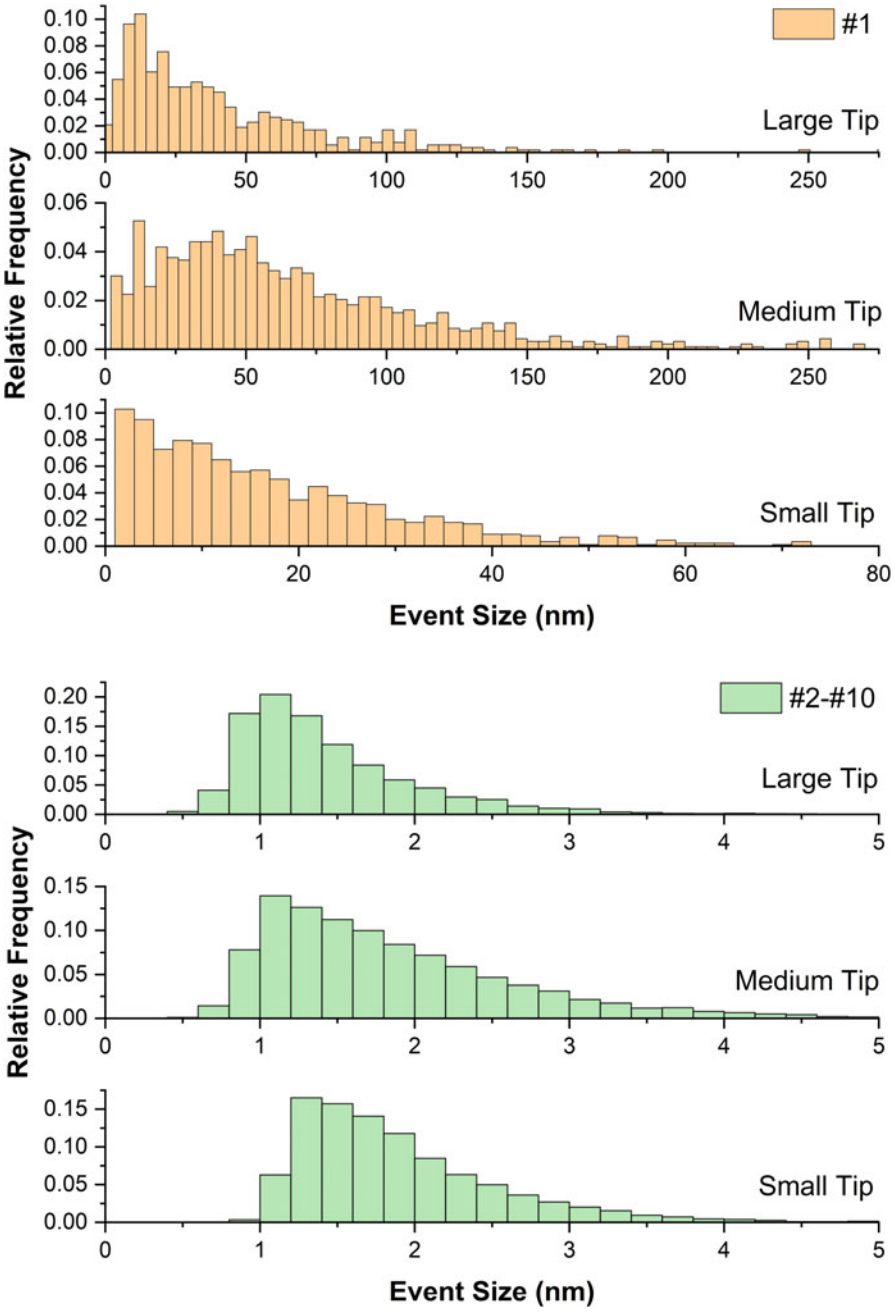

Figure 2: Histograms of displacement jump magnitudes for the first pop-in (#1) and higher-order pop-ins (#2–#10) across all three tip sizes.

that the finding of significantly different distributions found to describe plastic fluctuations in nanoindentation and microcrystal deformation is not due to different sampling rates. The same applies to the deformation rates, which in both cases remain largely below the critical rate expected for a soft fcc metal [32].

These differences between microcrystal deformation and nanoindentation are easily understood when considering that a substantial portion of the dislocation network evolution in microcrystals occurs prior to the break-away stress [46, 47, 48], which is defined as the point where considerable plastic strain is generated. Consequently, intermittency is observed in a regime of statistically unaltered dislocation density in a finite and constant volume. In the case of nanoindentation, higher-order pop-ins result from dislocation activity in an increasing plastic interaction volume and changing (geometrically necessary) dislocation density [49]. This clear loading-mode dependence of the event-size scaling reinforces nonuniversal intermittency in crystal plasticity [32, 33]. In fact, it shows how intermittent plasticity manifests itself not only as a scale-free-like and, thus,

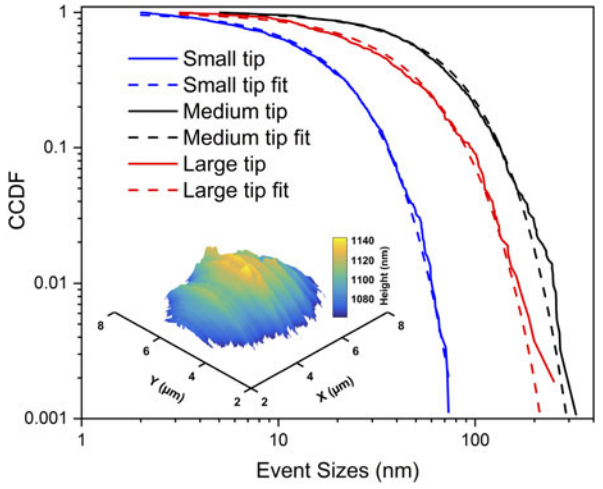

Figure 3: CCDFs of first-order event sizes for all tip sizes, with Weibull fits. Inset shows the topography of the large tip as measured by AFM, revealing local asperities at the highest points.

TABLE I: MLE fit parameters for event-size distributions from the experiments.

Event 1 (Weibull)	λ (nm)	β
Small tip	17.5 ± 1.2	1.19 ± 0.09
Medium tip	71.5 ± 2.8	1.32 ± 0.05
Large tip	42.0 ± 3.8	1.11 ± 0.08
Events 2–10 (Lognormal)	**μ (ln nm)**	**σ**
Small tip	0.337 ± 0.050	0.470 ± 0.035
Medium tip	0.378 ± 0.033	0.491 ± 0.027
Large tip	0.095 ± 0.056	0.450 ± 0.038
(Truncated power law)	**τ**	**x_0 (nm)**
Cu microcrystals	1.69 ± 0.05	421 ± 93

correlated process in microcrystal deformation, but also as a process with a well-defined scale in the case of nanoindentation. This scale is set by the indentation tip, and we note that the absence of scale invariance does not necessarily imply uncorrelated dislocation activity, for which Gaussian statistics is expected.

With increasing indentation depths, the surface irregularities of the large tip are expected to become less dominant since the tip more closely approximates a sphere. This is supported by the higher-order event statistics summarized in Fig. 4. The CCDFs of the higher-order pop-ins are found to be relatively similar for all tip sizes, with the exception that the large tip distribution of event sizes is shifted to slightly smaller sizes (reflected in the decreased value of μ for its lognormal distribution as seen in Table I). The small and medium tips are similar, except that the small tip shows a slight anomalous increase in the probability of event sizes in the 4–7 nm range. This may be related to the mechanism described by Xia et al. [43], where the pop-ins are more likely to follow a successive mode (multiple sequential pop-ins of moderate size) rather than the single pop-in mode (one very large plastic excursion) as the indenter tip radius decreases. In such a case, a sequence of pop-ins closely following one another in time might not be resolved as individual events, leading to an event-size increase that causes the shoulder in Fig. 4. Alternatively, a small fraction of the events of order #2 appearing in that particular CCDF may have recorded a very small first event, with event #2 more closely resembling the initial pop-ins from other indentation curves. This could, however, be excluded by further data analysis.

Stress statistics

Following the statistical analysis of the event sizes, we now turn our attention to the stress statistics of event order #1. The stresses at which the first pop-in occurs were determined by $\tau_{max} \approx 0.31(6PE^{*2})/(\pi^3R^2)^{1/3}$, with E^* being the effective indentation modulus, P being the load at the pop-in, and R being the radius of the tip [14]. When the various possible distribution functions of the MLE analysis are compared with the experimental data, it is found that the pop-in stresses of all tip sizes are very well described by both a lognormal distribution and a Weibull distribution. The MLE method returns a log likelihood ratio R of values (in order of tip size) 2.02, 2.13, and 3.01, and significance values (in order of tip size) of 0.044, 0.033, and 0.003, when comparing a lognormal distribution against a Weibull distribution. These numbers quantitatively underline the ambiguity, since a statistically significant difference between distributions is expected to return $R \gg 1$ and $P \ll 0.05$ [38, 39]. The fitting parameters for both distribution functions of event order #1 and all three tip sizes are listed in Table II. These numbers are somewhat sensitive to where the manually defined minimum x-value of the distribution is set, but no case strongly favoring one or the other distribution can be identified. This is also seen in Fig. 5, where the fitted distributions mainly reveal deviations in the high-valued tail structure of the data. We will later see that the experimental data suggests that the Weibull distribution is more likely. It should be noted that for the lognormal parameter μ, changing the units in which the distribution is numerically evaluated (e.g., from GPa to MPa) will significantly alter the central value (in the example given, increasing it by ln(1000) = 6.91) without numerically altering the width of the confidence interval. Therefore, the relative magnitudes of the central value and the width of the confidence interval should not be considered meaningful (e.g., in terms of "percent error"), although the absolute width of the interval has meaning. This also applies to the lognormal distributions in Table I.

Figure 5(a) visually presents the distribution CCDFs and Fig. 5(b) the histograms for the stresses at the initial pop-in. As

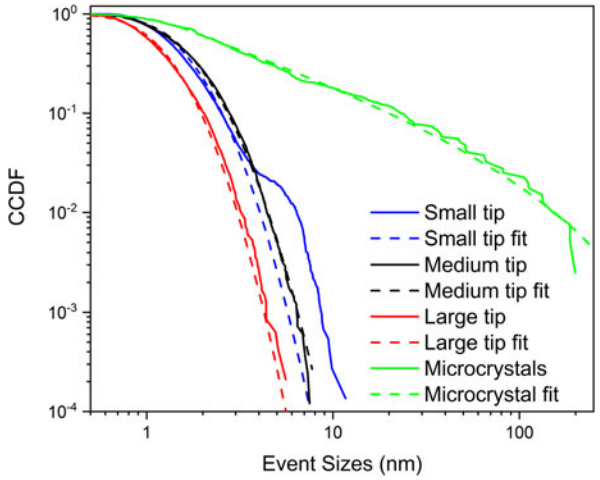

Figure 4: CCDFs of higher-order events #2–#10 for all tip sizes, with lognormal fits and data from microcrystal deformation that follows a truncated power law.

TABLE II: MLE fit parameters for the stresses of event order #1. Values for both a Lognormal and a Weibull distribution are listed.

Event 1 stress	Lognormal		Weibull	
	μ (ln GPa)	σ	λ (scale)	β (shape)
Small tip	0.587 ± 0.021	0.188 ± 0.016	1.929 ± 0.106	4.779 ± 0.753
Medium tip	−0.740 ± 0.016	0.238 ± 0.014	0.532 ± 0.020	4.280 ± 0.544
Large tip	−1.236 ± 0.018	0.195 ± 0.011	0.317 ± 0.026	5.082 ± 0.947

can be seen in the CCDF plots, all the tested indenter tips give relatively broad distributions of pop-in stresses. This is consistent with the work of Morris and Pharr et al. [22], where a tight distribution of stresses near the theoretical strength of the material for very small indenter tips (under 200 nm and much smaller than any of the tips used here) was observed. The same applies to low pop-in stresses for very large indenter tips (64–700 μm and much larger than any of the tips used here) [22]. For indenter tips of intermediate size, where the stressed volume is similar to the mean spacing between pre-existing defects, a broad distribution of pop-in stresses was found. These stress values are significantly above the bulk flow stress but well below the theoretical strength of the material. This matches the behavior seen here and rationalizes the gradual reduction in stress scale as a function of increasing tip size.

The stress scale of the first-order events (#1) in Fig. 5 is significantly different from any stresses related to events in the above-considered microcrystal experiment. A quantitative comparison can be made by taking 90% of the maximum stress under the indenter tip as an approximation of the stressed volume underneath the tip. We find that the mean stressed volume is 0.172 μm [3] for the small tip, 41.2 μm [3] for the medium tip, and 202 μm [3] for the large tip. The stress threshold of 90% was chosen to be similar to the stress ratio existing between the top and bottom of the microcrystal samples as a result of their slight taper. For all but the small tip, the obtained volumes are significantly larger than the nominal microcrystal volume of 18.8 μm [3]. Furthermore, the stress values at event initiation are all significantly higher than for any discrete displacement jump seen in the microcrystal experiment. For event order #1, the mean shear stress is 1.83 GPa for the small tip, 0.490 GPa for the medium tip, and 0.296 GPa for the large tip. In contrast, the mean stress is only 0.070 GPa (70 MPa) for slip events in the microcrystal sample, which in agreement with Ispanovity et al. [41], a distribute according to a Weibull distribution ($\lambda = 69.9$ and $\beta = 5.85$). The lack of comparable stress scales is again related to the aforementioned fact that intermittency is first observed when the microcrystal has experienced a strong increase in dislocation density prior to the break-away stress, whereas the indentation experiment with the tip sizes used here probes the activation of pre-existing dislocations in an as-grown crystal. It would, thus, be more meaningful to consider the stress scale of events #2–#10 in a comparison with a microcrystal, but unlike the case for the first pop-in, there exists no unique way to determine an estimate of the stress.

Assessing both the pop-in size and stress for event order #1 reveals a correlation, as shown in Fig. 6. For each tip in Fig. 6, an approximately linear correlation is found, where the slope scales with the tip size. Given that the distribution of first-order event sizes follows a Weibull distribution, whereas the MLE method did not yield a statistically significant result that could favor either a Weibull distribution or a lognormal distribution, we use the good linear correlation in Fig. 6 as an indication that the Weibull distribution indeed is a meaningful distribution function. Figure 6 further suggests that upon probing small volumes underneath the indenter tip, the pop-in stresses at #1 fluctuate largely because the low slope of the linear regression is only very weakly correlated with the size of the event. At the other extreme of the largest tip, the opposite is the case. We thus expect that there is no relationship between event size and stress when probing with even smaller or larger indentation probes. It must be kept in mind that this conclusion implies that the length scale of the pre-existing dislocation structure in the probed volume determines the scaling in Fig. 6 and not the size of the probed volume. Indeed, no such correlation exists in the before considered microcrystal deformation that has a volume approximately equivalent to the one probed with the smallest tip and also has a well-developed dislocation structure during intermittent plastic flow.

As a final part of this report, we will apply a recently proposed theoretical model for the statistical behavior of the stresses for the first pop-in [36]. This starts with the assumption that the material contains a number of flaws M that can trigger deformation at activation stresses having a power-law

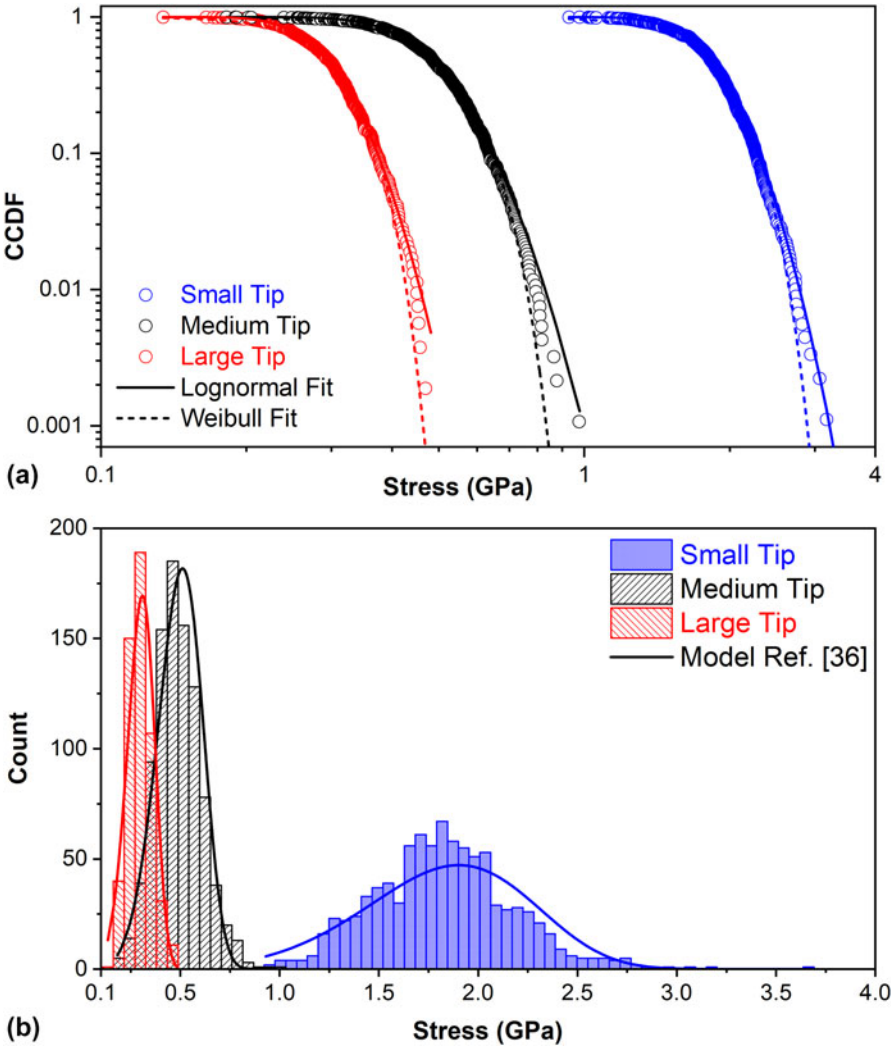

Figure 5: (a) CCDF of the maximum stress underneath the indenter tip for the first pop-in event across all tip sizes on a log–log plot. Both a lognormal fit and a Weibull fit, using the parameters summarized in Table II are shown. (b) Histogram of the same data on a linear plot with lines being the statistical prediction (not fit) derived on the bases of the model from Ref. 36.

distribution $P(\sigma) \sim \sigma^{\alpha}$. If the number of critical stresses in a stressed volume V is large, then the observed stress at the first pop-in σ_1 will be primarily dependent on the low-end tail behavior of the positively valued distribution $P(\sigma)$. This type of weakest-link effect can be shown to consistently produce a distribution of observed first pop-in stresses $P_M(\sigma_1)$ with the form of a Weibull distribution, regardless of the nature of the material's flaw-strength distribution $P(\sigma)$, although the latter can affect the shape and scale parameters of the resulting Weibull distribution.

Sampling a finite number of critical stresses M in a volume with a volumetric flaw density ρ, this can be related to the stressed volume as $M = \rho V$. Derlet and Maaß [36] showed that the mean stress at the first pop-in versus the stressed volume is predicted to follow a power-law relation with scaling exponent $\gamma = (1 + \alpha)^{-1}$, where $1/\gamma = \beta$ is the Weibull shape parameter for $P_M(\sigma_1)$ [36]. This allows plotting the mean stress at the first pop-in, σ_1 versus the indenter-tip radius, equivalent to assuming $V = r^3$. Figure 7 displays the original data from Ref. 22, including the power-law fit from the model in Ref. 36, and the data obtained in this work.

Following the previously derived conclusion that the stress variation of the first pop-in is best described by a Weibull distribution, the values in Table II can now be compared with the value of a Weibull shape parameter obtained from the data in Fig. 7. Accordingly, the scaling exponent is found to be 0.597. With the relationship between average stress and indenter volume ($\sim r^3$), the scaling exponent becomes $\gamma = 0.597/3$, which yields a shape parameter of $1/0.199 = \beta = 5.025$. This value is in good agreement with the values listed in Table II. Furthermore, the accuracy of this theoretical result can be tested by plotting Eq. (1) with the here found shape parameter and the scale parameters as given by the characteristic stress

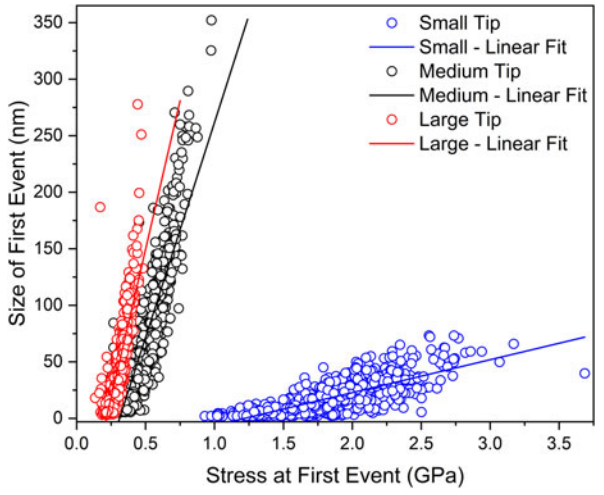

Figure 6: Correlation between the size of event #1 and the stress at which it occurs.

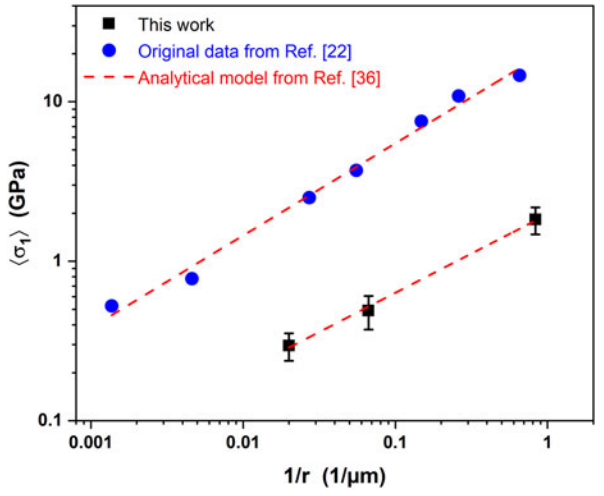

Figure 7: Average first critical stress from indentation data obtained with different tip sizes. Circles are data points from Ref. 22 and squares from this work. The lines are a fit of a derived power law from Ref. 36. Reprinted from Ref. 36, with the permission of AIP Publishing.

[36], σ_1^*, which is found via $\langle\sigma_1\rangle/\Gamma(1+\gamma)$, where Γ is the gamma function. These curves are shown in Fig. 5(b), demonstrating a very good agreement, and any remaining inaccuracy in the theoretical prediction could plausibly be attributed to the weak statistical significance of favoring a Weibull distribution over a lognormal distribution. The model thus allows determining any average first critical stress, and therefore the full Weibull distribution, for any other tip size. Finally, the material's true flaw-strength distribution $P(\sigma)$ can be obtained from the same model outlined in Ref. 36 by taking into account that the power-law exponent α needs to be corrected for the indenter geometry since the probed plastic volume scales with indenter depth and, therefore, the stress level. This was shown to result in $\alpha_{true} = \alpha - 3 \approx 1.03$, which is a value somewhat larger than that reported for 2D and 3D dislocation dynamics simulations [41, 42].

Summary

In this study, we have investigated the statistics of pop-in magnitudes and stresses during nanoindentation on pure single crystalline Cu with different probe sizes. Irrespective of the indentation tip size, both the stresses and the magnitudes of the first discrete plastic event (pop-in) are very well captured by a Weibull model. Subsequent plastic events admit magnitudes that are distributed according to lognormal statistics, irrespective of orders #2–#10 analyzed here. This contrasts strongly with the current focus of power-law–distributed plastic events obtained during microcrystal deformation, which indicates correlated dislocation activity that is free of a particular length scale. Given the abrupt plastic events and their large magnitudes, we believe that even if scale invariance is absent, correlated dislocation activity still persists in the highly stressed region underneath the indentation tip. Only pure Gaussian statistics could be taken as an indication for uncorrelated dislocation activity. More generally, these results indicate how the stochastic evolution of a stressed dislocation network can follow very different statistics depending on the loading mode.

Methodology

All nanoindentation experiments were performed on ⟨001⟩-oriented bulk single crystalline Cu that was grown from the melt using the Czochralski method. Laue diffraction patterns were used to create ⟨001⟩ and ⟨111⟩ pole figures showing the accuracy of the nominal out-of-plane orientation to be well within one degree. The test specimen surface was mechanically ground and polished before being electropolished using the procedure outlined in Ref. 50. Nanoindentation was conducted with conospherical tips of nominal radii 1.2, 15, and 50 μm. Nominal tip sizes were verified with both optical and scanning electron microscopy. The indentation tests were performed with a Hysitron TI-950, and a Hysitron Picoindenter PI-85 using automated methods was used to run square arrays. The tests were run in force-controlled mode with a loading rate of 0.3–1.5 nm/s, and the data acquisition rate was 20 Hz. For each tip size, the indent spacing was adjusted to be five times the projected indent width. More than 500 indents were made with each tip size.

The resulting force–displacement data were analyzed using custom Matlab routines to determine and record the details of the first ten pop-ins (#1–#10). The routine evaluated locally the slope of the force–displacement trace to first identify the approximate location of a pop-in. Subsequently, a maximum in the point-wise displacement change located the displacement jump more precisely, and the displacements at plus or

minus a value equal to the standard deviation of the force values were used to define the starting and stopping positions of the displacement jump. The procedure needed to be adapted to each tip size to match the noise structure of the experimental data. Figure 1 displays a typical indentation force–displacement curve that was recorded using the smallest tip. Using this numerical method, the force and displacement at which a pop-in occurs, as well as its size, was obtained for further statistical evaluation. Figure 1 also displays a Hertzian fit-line to the initial part of the indentation curve prior to the first pop-in.

Acknowledgments

This research was carried out in part in the Frederick Seitz Materials Research Laboratory Central Research Facilities, University of Illinois. R.M. is grateful for financial support by the NSF CAREER program (grant NSF DMR 1654065), and for start-up funds provided by the Department of Materials Science and Engineering at UIUC. The authors also thank J. Spears for conducting AFM measurements.

References

1. **R. Maass and P.M. Derlet**: Micro-plasticity and recent insights from intermittent and small-scale plasticity. *Acta Mater.* **143**, 338 (2018).
2. **A. Vandenbeukel**: Theory of effect of dynamic strain aging on mechanical properties. *Phys. Status Solidi A* **30**, 197 (1975).
3. **R.A. Mulford and U.F. Kocks**: New observations on the mechanisms of dynamic strain-aging and of jerky flow. *Acta Metall.* **27**, 1125 (1979).
4. **H.Y. Yasuda, K. Shigeno, and T. Nagase**: Dynamic strain aging of $Al_{0.3}$CoCrFeNi high entropy alloy single crystals. *Scr. Mater.* **108**, 80 (2015).
5. **R. Maass and J.F. Löffler**: Shear-band dynamics in metallic glasses. *Adv. Funct. Mater.* **25**, 2353 (2015).
6. **E. Schmid and M.A. Valouch**: About the sudden translation of zinc crystals. *Z. Phys.* **75**, 531 (1932).
7. **R. Becker and E. Orowan**: Sudden expansion of zinc crystals. *Z. Phys.* **79**, 566 (1932).
8. **R.F. Tinder and J.P. Trzil**: Millimicroplastic burst phenomena in zinc monocrystals. *Acta Metall.* **21**, 975 (1973).
9. **M.D. Uchic, P.A. Shade, and D.M. Dimiduk**: Plasticity of micrometer-scale single-crystals in compression. *Annu. Rev. Mater. Sci.* **39**, 361 (2009).
10. **G. Sparks, Y. Cui, G. Po, Q. Rizzardi, J. Marian, and R. Maass**: Avalanche statistics and the intermittent-to-smooth transition in microplasticity. *Phys. Rev. Mater.* **3**, 080601 (2019).
11. **E.T. Lilleodden and W.D. Nix**: Microstructural length-scale effects in the nanoindentation behavior of thin gold films. *Acta Mater.* **54**, 1583 (2006).
12. **D. Lorenz, A. Zeckzer, U. Hilpert, P. Grau, H. Johansen, and H.S. Leipner**: Pop-in effect as homogeneous nucleation of dislocations during nanoindentation. *Phys. Rev. B* **67**, 172101 (2003).
13. **O.L. Warren, S.A. Downs, and T.J. Wyrobek**: Challenges and interesting observations associated with feedback-controlled nanoindentation. *Z. Metallkd.* **95**, 287 (2004).
14. **S. Shim, H. Bei, E.P. George, and G.M. Pharr**: A different type of indentation size effect. *Scr. Mater.* **59**, 1095 (2008).
15. **J.C. Crone, L.B. Munday, J.J. Ramsey, and J. Knap**: Modeling the effect of dislocation density on the strength statistics in nanoindentation. *Modell. Simul. Mater. Sci. Eng.* **26**, 015009 (2017).
16. **A. Barnoush, M.T. Welsch, and H. Vehoff**: Correlation between dislocation density and pop-in phenomena in aluminum studied by nanoindentation and electron channeling contrast imaging. *Scr. Mater.* **63**, 465 (2010).
17. **L. Zhang and T. Ohmura**: Plasticity initiation and evolution during nanoindentation of an iron–3% silicon crystal. *Phys. Rev. Lett.* **112** (2014).
18. **P. Sudharshan Phani, K.E. Johanns, E.P. George, and G.M. Pharr**: A stochastic model for the size dependence of spherical indentation pop-in. *J. Mater. Res.* **28**, 2728 (2013).
19. **C.A. Schuh, J.K. Mason, and A.C. Lund**: Quantitative insight into dislocation nucleation from high-temperature nanoindentation experiments. *Nat. Mater.* **4**, 617 (2005).
20. **C.A. Schuh and A.C. Lund**: Application of nucleation theory to the rate dependence of incipient plasticity during nanoindentation. *J. Mater. Res.* **19**, 2152 (2004).
21. **Y.L. Chiu and A.H.W. Ngan**: Time-dependent characteristics of incipient plasticity in nanoindentation of a Ni_3Al single crystal. *Acta Mater.* **50**, 1599 (2002).
22. **J.R. Morris, H. Bei, G.M. Pharr, and E.P. George**: Size effects and stochastic behavior of nanoindentation pop in. *Phys. Rev. Lett.* **106**, 165502 (2011).
23. **D.M. Dimiduk, C. Woodward, R. LeSar, and M.D. Uchic**: Scale-free intermittent flow in crystal plasticity. *Science* **312**, 1188 (2006).
24. **F.F. Csikor, C. Motz, D. Weygand, M. Zaiser, and S. Zapperi**: Dislocation avalanches, strain bursts, and the problem of plastic forming at the micrometer scale. *Science* **318**, 251 (2007).
25. **M. Zaiser, J. Schwerdtfeger, A.S. Schneider, C.P. Frick, B.G. Clark, P.A. Gruber, and E. Arzt**: Strain bursts in plastically deforming molybdenum micro- and nanopillars. *Philos. Mag.* **88**, 3861 (2008).
26. **R. Maass, P.M. Derlet, and J.R. Greer**: Independence of slip velocities on applied stress in small crystals. *Small* **11**, 341 (2015).
27. **N. Friedman, A.T. Jennings, G. Tsekenis, J-Y. Kim, M. Tao, J.T. Uhl, J.R. Greer, and K.A. Dahmen**: Statistics of dislocation slip avalanches in nanosized single crystals show tuned critical behavior predicted by a simple mean field model. *Phys. Rev. Lett.* **109**, 095507 (2012).

28. **M. LeBlanc, L. Angheluta, K. Dahmen, and N. Goldenfeld**: Universal fluctuations and extreme statistics of avalanches near the depinning transition. *Phys. Rev. E* **87**, 022126 (2013).
29. **J.P. Sethna, M.K. Bierbaum, K.A. Dahmen, C.P. Goodrich, J.R. Greer, L.X. Hayden, J.P. Kent-Dobias, E.D. Lee, D.B. Liarte, X. Ni, K.N. Quinn, A. Raju, D.Z. Rocklin, A. Shekhawat, and S. Zapperi**: Deformation of crystals: Connections with statistical physics. *Annu. Rev. Mater. Res.* **47**, 217 (2017).
30. **J.T. Uhl, S. Pathak, D. Schorlemmer, X. Liu, R. Swindeman, B.A.W. Brinkman, M. LeBlanc, G. Tsekenis, N. Friedman, R. Behringer, D. Denisov, P. Schall, X. Gu, W.J. Wright, T. Hufnagel, A. Jennings, J.R. Greer, P.K. Liaw, T. Becker, G. Dresen, and K.A. Dahmen**: Universal quake statistics: From compressed nanocrystals to earthquakes. *Sci. Rep.* **5**, 16493 (2015).
31. **G. Sparks and R. Maass**: Shapes and velocity relaxation of dislocation avalanches in Au and Nb microcrystals. *Acta Mater.* **152**, 86 (2018).
32. **G. Sparks and R. Maass**: Nontrivial scaling exponents of dislocation avalanches in microplasticity. *Phys. Rev. Mater.* **2**, 120601 (2018).
33. **G. Sparks and R. Maass**: Effects of orientation and pre-deformation on velocity profiles of dislocation avalanches in gold microcrystals. *Eur. Phys. J. B* **92**, 15 (2019).
34. **T. Niiyama and T. Shimokawa**: Atomistic mechanisms of intermittent plasticity in metals: Dislocation avalanches and defect cluster pinning. *Phys. Rev. E* **91**, 022401 (2015).
35. **L.M. Brown**: Power laws in dislocation plasticity. *Philos. Mag.* **96**, 2696 (2016).
36. **P.M. Derlet and R. Maass**: The stress statistics of the first pop-in or discrete plastic event in crystal plasticity. *J. Appl. Phys.* **120**, 225101 (2016).
37. **R. Maass, M. Wraith, J.T. Uhl, J.R. Greer, and K.A. Dahmen**: Slip statistics of dislocation avalanches under different loading modes. *Phys. Rev. E* **91**, 042403 (2015).
38. **J. Alstott, E. Bullmore, and D. Plenz**: Powerlaw: A Python package for analysis of heavy-tailed distributions. *PLoS One* **9**, e85777 (2014).
39. **A. Clauset, C.R. Shalizi, and M.E.J. Newman**: Power-law distributions in empirical data. *SIAM Rev.* **51**, 661 (2009).
40. **R. Maass, C.A. Volkert, and P.M. Derlet**: Crystal size effect in two dimensions—Influence of size and shape. *Scr. Mater.* **102**, 27 (2015).
41. **P.D. Ispanovity, A. Hegyi, I. Groma, G. Gyoergyi, K. Ratter, and D. Weygand**: Average yielding and weakest link statistics in micron-scale plasticity. *Acta Mater.* **61**, 6234 (2013).
42. **P.D. Ispánovity, D. Tüzes, P. Szabó, M. Zaiser, and I. Groma**: Role of weakest links and system-size scaling in multiscale modeling of stochastic plasticity. *Phys. Rev. B* **95**, 054108 (2017).
43. **Y. Xia, Y. Gao, G.M. Pharr, and H. Bei**: Single versus successive pop-in modes in nanoindentation tests of single crystals. *J. Mater. Res.* **31**, 2065 (2016).
44. **S. Papanikolaou, Y. Cui, N. Ghoniem**: Avalanches and plastic flow in crystal plasticity: An overview. *Modell. Simul. Mater. Sci. Eng.* **26**, 013001 (2018).
45. **M. LeBlanc, A. Nawano, W.J. Wright, X. Gu, J.T. Uhl, and K.A. Dahmen**: Avalanche statistics from data with low time resolution. *Phys. Rev. E* **94**, 052135 (2016).
46. **D.M. Norfleet, D.M. Dimiduk, S.J. Polasik, M.D. Uchic, and M.J. Mills**: Dislocation structures and their relationship to strength in deformed nickel microcrystals. *Acta Mater.* **56**, 2988 (2008).
47. **R. Maass and M.D. Uchic**: In situ characterization of the dislocation-structure evolution in Ni micro-pillars. *Acta Mater.* **60**, 1027 (2012).
48. **S.H. Oh, M. Legros, D. Kiener, and G. Dehm**: In situ observation of dislocation nucleation and escape in a submicrometre aluminium single crystal. *Nat. Mater.* **8**, 95 (2009).
49. **N. Zaafarani, D. Raabe, F. Roters, and S. Zaefferer**: On the origin of deformation-induced rotation patterns below nanoindents. *Acta Mater.* **56**, 31 (2008).
50. **F.I. Metz**: Electropolishing of metals. Retrospective theses and dissertations, Iowa State University, Paper 2622, 1960.